

Kinetic temperature of massive star forming molecular clumps measured with formaldehyde. II. The Large Magellanic Cloud

X. D. Tang^{1,2,3}, C. Henkel^{1,4}, C. -H. R. Chen¹, K. M. Menten¹, R. Indebetouw^{5,6}, X. W. Zheng⁷, J. Esimbek^{2,3}, J. J. Zhou^{2,3}, Y. Yuan^{2,3}, D. L. Li^{2,3}, and Y. X. He^{2,3}

¹ Max-Planck-Institut für Radioastronomie, Auf dem Hügel 69, 53121 Bonn, Germany
e-mail: xdtang@mpi-fr-bonn.mpg.de

² Xinjiang Astronomical Observatory, Chinese Academy of Sciences, 830011 Urumqi, China

³ Key Laboratory of Radio Astronomy, Chinese Academy of Sciences, 830011 Urumqi, China

⁴ Astronomy Department, King Abdulaziz University, PO Box 80203, 21589 Jeddah, Saudi Arabia

⁵ National Radio Astronomy Observatory, 520 Edgemont Rd, Charlottesville, VA 22903, USA

⁶ University of Virginia, Charlottesville, VA 22903, USA

⁷ Department of Astronomy, Nanjing University, 210093 Nanjing, China

January 7, 2022

ABSTRACT

Context. The kinetic temperature of molecular clouds is a fundamental physical parameter affecting star formation and the initial mass function. The Large Magellanic Cloud (LMC), the closest star forming galaxy with low metallicity, provides an ideal laboratory to study star formation in such an environment.

Aims. The classical dense molecular gas thermometer NH_3 is rarely available in a low metallicity environment because of photoionization and a lack of nitrogen atoms. Our goal is to directly measure the gas kinetic temperature with formaldehyde toward six star-forming regions in the LMC.

Methods. Three rotational transitions ($J_{\text{K}_A\text{K}_C} = 3_{03-2_{02}}$, $3_{22-2_{21}}$, and $3_{21-2_{20}}$) of para- H_2CO near 218 GHz were observed with the Atacama Pathfinder Experiment (APEX) 12 m telescope toward six star forming regions in the LMC. Those data are complemented by C^{18}O 2-1 spectra.

Results. Using non-LTE modeling with RADEX, we derive the gas kinetic temperature and spatial density, using as constraints the measured para- H_2CO $3_{21-2_{20}}/3_{03-2_{02}}$ and para- H_2CO $3_{03-2_{02}}/\text{C}^{18}\text{O}$ 2-1 ratios. Excluding the quiescent cloud N159S, where only one para- H_2CO line could be detected, the gas kinetic temperatures derived from the preferred para- H_2CO $3_{21-2_{20}}/3_{03-2_{02}}$ line ratios range from 35 to 63 K with an average of 47 ± 5 K (errors are unweighted standard deviations of the mean). Spatial densities of the gas derived from the para- H_2CO $3_{03-2_{02}}/\text{C}^{18}\text{O}$ 2-1 line ratios yield $0.4 - 2.9 \times 10^5 \text{ cm}^{-3}$ with an average of $1.5 \pm 0.4 \times 10^5 \text{ cm}^{-3}$. Temperatures derived from the para- H_2CO line ratio are similar to those obtained with the same method from Galactic star forming regions and agree with results derived from CO in the dense regions ($n(\text{H}_2) > 10^3 \text{ cm}^{-3}$) of the LMC. A comparison of kinetic temperatures derived from para- H_2CO with those from the dust also shows good agreement. This suggests that the dust and para- H_2CO are well mixed in the studied star forming regions. A comparison of kinetic temperatures derived from para- H_2CO $3_{21-2_{20}}/3_{03-2_{02}}$ and $\text{NH}_3(2,2)/(1,1)$ shows, however, a drastic difference. In the star forming region N159W, the gas temperature derived from the $\text{NH}_3(2,2)/(1,1)$ line ratio is ~ 16 K (Ott et al. 2010), which is only half the temperature derived from para- H_2CO and the dust. Furthermore, ammonia shows a very low abundance in a $30''$ beam. Apparently, ammonia only survives in the most shielded pockets of dense gas not yet irradiated by UV photons, while formaldehyde, less affected by photodissociation, is more widespread and is also sampling regions more exposed to the radiation of young massive stars. A correlation between the gas kinetic temperatures derived from para- H_2CO and infrared luminosity, represented by the $250 \mu\text{m}$ flux, suggests that the kinetic temperatures traced by para- H_2CO are correlated with the ongoing massive star formation in the LMC.

Key words. Galaxies: star formation – Galaxies: Magellanic Clouds – Galaxies: ISM – Galaxies: irregular – ISM: molecules – radio lines: ISM

1. Introduction

The Large Magellanic Cloud (LMC), at a distance of ~ 50 kpc (Pietrzyński et al. 2013), is the nearest low metallicity (Rolleston 2002) star-forming galaxy to the Milky Way. The relatively face-on view offered by the LMC provides an ideal

perspective to study star formation, particularly massive star formation associated with its numerous stellar clusters. In the LMC, the FUV field is stronger than in the Milky Way (Westerlund 1990). It is thus well suited to study the properties of the interstellar medium, the evolution of molecular clouds, and star for-

mation in an active low metallicity galaxy, also providing a link to galaxies at high redshift.

The physical properties of the molecular gas in the LMC, in particular the kinetic temperature, are not well constrained. The easily thermalized and optically thick rotational CO transitions are good temperature tracers of the cold and dense gas in local clouds. Generally, however, they often suffer from a lack of information on the beam filling factor in extragalactic clouds. Multi-level observations of suitable molecules deliver the most reliable temperature determinations. The metastable lines of ammonia (NH_3) are frequently used as the standard molecular cloud thermometer in molecular clouds within our Galaxy and also in external galaxies (Ho & Townes 1983; Walmsley & Ungerechts 1983; Danby et al. 1988; Henkel et al. 2000, 2008; Weiß et al. 2001; Mauersberger et al. 2003; Ao et al. 2011; Lebrón et al. 2011; Ott et al. 2011; Wienen et al. 2012; Mangum et al. 2013a). However, the ammonia abundance can vary strongly in different molecular environments (e.g., 10^{-5} in dense, molecular “hot cores” around newly formed massive stars, Mauersberger et al. 1987; 10^{-8} in dark clouds, Benson & Myers 1983; Chira et al. 2013; 10^{-10} in a massive star forming cloud of the LMC, Ott et al. 2010) and is extremely affected by a high UV flux. Thus, in a low metallicity environment with high UV flux and a lack of shielding dust grains, ammonia is of limited use as a reliable probe to trace the gas kinetic temperature. To make this problem even more severe, the LMC is also a galaxy with particularly low nitrogen abundance ($\sim 10\%$ solar, Wang et al. 2009; Ott et al. 2010).

Formaldehyde (H_2CO) is a ubiquitous molecule in the Galactic interstellar medium (ISM) of our and external galaxies (Downes et al. 1980; Cohen & Few 1981; Bieging et al. 1982; Cohen et al. 1983; Baan et al. 1986, 1990, 1993; Henkel et al. 1991; Zylka et al. 1992; Hüttemeister et al. 1997; Heikkilä et al. 1999; Wang et al. 2004, 2009; Mangum et al. 2008; Zhang et al. 2012; Mangum et al. 2013b; Ao et al. 2013; Tang et al. 2013; Ginsburg et al. 2015, 2016; Guo et al. 2016). H_2CO is thought to be formed on the surface of dust grains by successive hydrogenation of CO (Watanabe & Kouchi 2002; Woon 2002; Hidaka et al. 2004): $\text{CO} \rightarrow \text{HCO} \rightarrow \text{H}_2\text{CO}$. Variations of the fractional abundance of H_2CO do not exceed one order of magnitude. For example, the fractional abundance of H_2CO is similar across various sub regions of the well-studied Orion-KL nebula, i.e., the “hot core” and the “compact ridge” (Mangum et al. 1990, 1993; Caselli et al. 1993; Johnstone et al. 2003).

Para- H_2CO has a rich variety of millimeter and submillimeter transitions. Line ratios of para- H_2CO involving different K_a ladders are good tracers of the kinetic temperature, such as para- H_2CO $J_{K_a K_c} = 3_{22-2_{21}}/3_{03-2_{02}}$, $4_{23-3_{22}}/4_{04-3_{03}}$, and $5_{23-4_{22}}/5_{05-4_{04}}$, since the relative populations of the K_a ladders of para- H_2CO are predominantly governed by collisions (Mangum & Wootten 1993; Mühle et al. 2007). Among these para- H_2CO lines, the above three transitions with rest frequencies of 218.222, 218.475, and 218.760 GHz, respectively, are particularly useful for use a thermometer, because they are strong enough for extragalactic observations and because they can be measured simultaneously within a bandwidth of 1 GHz. Temperature determined from these ratios are free from uncertainties related to pointing accuracy, calibration or different beam sizes. Since the line emission is optically thin and the levels are located up to 68 K above the ground state, the line ratios are sensitive to gas kinetic temperatures up to 50 K with relatively small uncertainties (Mangum & Wootten

Table 1. Source coordinates, integration times, and epochs.

Sources	RA(J2000) h m s	DEC(J2000) ° ' "	Int. Time min	Obs. Date
N159W	05:39:35.2	-69:45:37.0	229	July-2008
N113	05:13:17.2	-69:22:23.0	91	September-2008
N44BC	05:22:02.8	-67:57:45.8	68	May-2014
30 Dor	05:38:49.3	-69:04:44.0	64	May-2014
N159S	05:40:02.8	-69:50:32.7	166	May-July-2014
N159E	05:40:04.4	-69:44:34.0	80	July-2014

1993; Ao et al. 2013). Para- H_2CO 3–2 line ratios have been used to measure the molecular gas kinetic temperatures in our Galactic center (Qin et al. 2008; Ao et al. 2013; Johnston et al. 2014; Ginsburg et al. 2016; Immer et al. 2016), star formation regions (Mangum & Wootten 1993; Mitchell et al. 2001; Watanabe & Mitchell 2008; Tang et al. 2016), as well as in external galaxies (e.g., Mühle et al. 2007).

Multitransition observations of molecular clouds in the LMC (Johansson et al. 1998; Heikkilä et al. 1999; Israel et al. 2003; Kim et al. 2004; Bolatto et al. 2005; Pineda et al. 2008; Mizuno et al. 2010; Minamidani et al. 2008, 2011; Fujii et al. 2014; Paron et al. 2016) suggest that the molecular gas traced by CO may be warmer and/or denser than in our Galaxy. $\text{NH}_3(1,1)$ and (2,2) lines have been surveyed toward seven star-forming regions in the LMC by Ott et al. (2010) using the Australia Telescope Compact Array (ATCA). Emission is only detected in the massive star-forming region N159W. This represents so far the only detection of NH_3 in the Magellanic Clouds. The gas kinetic temperature derived from $\text{NH}_3(2,2)/(1,1)$ is cold (~ 16 K), which is two times lower than the derived dust temperature 30 – 40 K (Heikkilä et al. 1999; Bolatto et al. 2000; Gordon et al. 2014). Ott et al. (2010) also found a low fractional NH_3 abundance of $\sim 4 \times 10^{-10}$, which is lower by 1.5 – 5 orders of magnitude than those observed in Galactic star-forming regions. Previous observations of formaldehyde have been made in the LMC (e.g., Whiteoak & Gardner 1976; Johansson et al. 1994; Heikkilä et al. 1999; Wang et al. 2009) and H_2CO has been detected in many dense clumps. These observations show that the fractional abundance of para- H_2CO ranges from 1 to 6×10^{-10} , which agrees with the values found in our Galactic molecular clouds (e.g., Güsten & Henkel 1983; Zylka et al. 1992; Johnstone et al. 2003; Ao et al. 2013; Tang et al. 2016).

For this paper, we have carried out deep observations of the six star forming regions 30 Dor, N44BC, N113, N159E, N159S, and N159W in the LMC. Targeting three transitions of para- H_2CO ($J_{K_a K_c} = 3_{03-2_{02}}$, $3_{22-2_{21}}$, and $3_{21-2_{20}}$) as well as C^{18}O 2-1 we simultaneously determine kinetic temperatures and spatial densities at high precision. In Sections 2 and 3, we introduce our observations of the para- H_2CO triplet and the data reduction, and describe the main results. These are then discussed in Section 4. Our main conclusions are summarized in Section 5.

2. Observations and data reduction

Our observations were carried out in 2008 and 2014 (summarized in Table 1) with the Atacama Pathfinder Experiment (APEX) 12 m telescope located on Chajnantor (Chile) using the APEX-1 (SHEFI) receiver. The beam size is $\sim 30''$ (~ 7 pc at 50 kpc distance) at 218 GHz. The main beam efficiency and the forward efficiency were 0.75 and 0.97, respectively. N113 and N159W were observed in 2008 with an old Fast Fourier Transform Spectrometer (FFTS), which consists of two units with a bandwidth of 1 GHz each and a velocity resolution of 0.1675

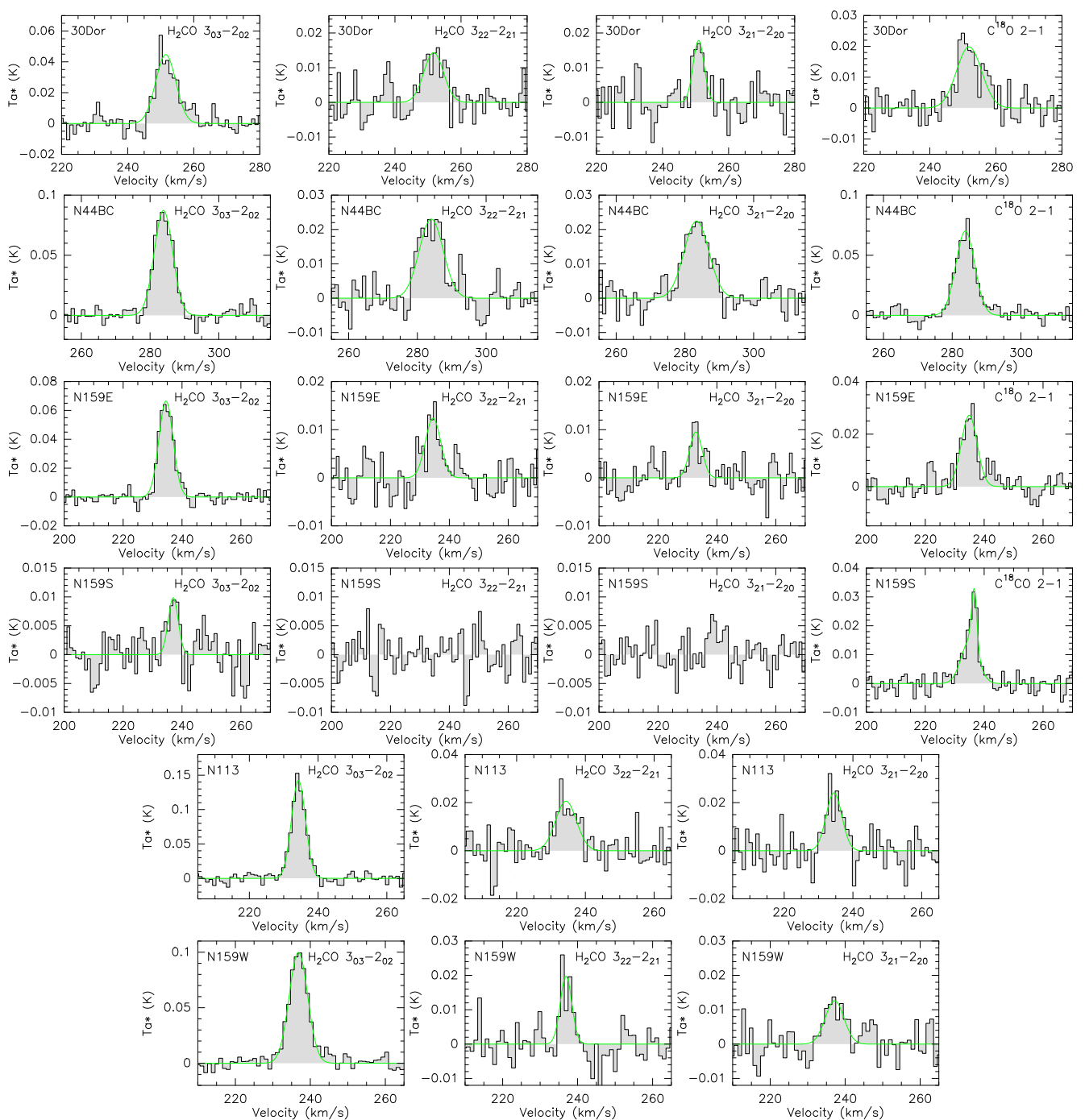


Fig. 1. Para-H₂CO ($3_{03}-2_{02}$, $3_{22}-2_{21}$, and $3_{21}-2_{20}$) and C¹⁸O (2-1) spectra.

km s⁻¹. The frequency is centered at 218.480 GHz. Our data includes all three of the 218 GHz para-H₂CO lines. 30 Dor, N159E, N159S, and N44BC were observed in 2014. Here we used the new eXtended bandwidth Fast Fourier Transform Spectrometer (XFFTS) backend with two spectral windows of 2.5 GHz bandwidth and a velocity resolution of 0.1047 km s⁻¹. The central frequency is set at 218.550 GHz. These data do not only include the three para-H₂CO lines but also the 219.560 GHz C¹⁸O (2-1) transition.

Toward each of the six star forming regions in the LMC Wong et al. (2011) took a single pointing, high sensitivity (~5 mK rms, T_{mb} scale, beam size ~30'') spectrum centered on its

CO emission peak which will be used to estimate $N(\text{H}_2)$ in Section 4.1. Ancillary C¹⁸O 2-1 data have been published by Heikkilä et al. (1998) and Wang et al. (2009). In addition, ammonia (NH₃) data from the LMC (Ott et al. 2010) and Herschel infrared data will also play an important role.

Data reduction for spectral lines was performed using CLASS from the GILDAS package¹. To enhance signal to noise ratios (S/N) in individual channels, we smoothed contiguous channels to a velocity resolution of ~1.0 km s⁻¹. Sources observed are listed in Table 1.

¹ <http://www.iram.fr/IRAMFR/GILDAS>

Table 2. Para-H₂CO and C¹⁸O spectral parameters^a.

Sources	Molecule	Transition	$\int T_{\text{mb}} dv$ K km s ⁻¹	V_{lsr} km s ⁻¹	FWHM ^b km s ⁻¹	T_{mb} K	rms mK
30 Dor	H ₂ CO	3 ₀₃ – 2 ₀₂	0.401 (0.026)	250.92 (0.21)	6.12 (0.47)	0.061	6.8
	H ₂ CO	3 ₂₂ – 2 ₂₁	0.114 (0.023)	251.61 (0.70)	6.48 (1.19)	0.017	6.5
	H ₂ CO	3 ₂₁ – 2 ₂₀	0.109 (0.021)	251.01 (0.41)	4.29 (1.00)	0.023	6.4
	C ¹⁸ O	2 – 1	0.190 (0.026)	251.25 (0.48)	7.09 (1.34)	0.025	5.6
N113	H ₂ CO	3 ₀₃ – 2 ₀₂	0.930 (0.029)	234.25 (0.07)	4.86 (0.17)	0.181	7.0
	H ₂ CO	3 ₂₂ – 2 ₂₁	0.217 (0.035)	234.40 (0.58)	7.05 (1.20)	0.029	6.9
	H ₂ CO	3 ₂₁ – 2 ₂₀	0.213 (0.025)	234.36 (0.33)	5.69 (0.68)	0.035	7.3
N44BC	H ₂ CO	3 ₀₃ – 2 ₀₂	0.775 (0.026)	283.86 (0.11)	6.37 (0.23)	0.114	6.5
	H ₂ CO	3 ₂₂ – 2 ₂₁	0.155 (0.019)	283.97 (0.45)	6.98 (0.88)	0.021	5.2
	H ₂ CO	3 ₂₁ – 2 ₂₀	0.152 (0.021)	283.45 (0.47)	6.50 (0.90)	0.022	5.1
	C ¹⁸ O	2 – 1	0.558 (0.022)	283.78 (0.12)	6.08 (0.28)	0.086	6.2
N159W	H ₂ CO	3 ₀₃ – 2 ₀₂	0.788 (0.019)	236.78 (0.07)	5.82 (0.17)	0.127	6.2
	H ₂ CO	3 ₂₂ – 2 ₂₁	0.101 (0.017)	237.00 (0.30)	3.65 (0.70)	0.026	6.4
	H ₂ CO	3 ₂₁ – 2 ₂₀	0.105 (0.017)	236.98 (0.53)	5.94 (1.00)	0.017	5.2
N159E	H ₂ CO	3 ₀₃ – 2 ₀₂	0.555 (0.017)	234.53 (0.09)	5.84 (0.21)	0.090	4.9
	H ₂ CO	3 ₂₂ – 2 ₂₁	0.112 (0.018)	234.45 (0.47)	6.46 (1.37)	0.016	4.3
	H ₂ CO	3 ₂₁ – 2 ₂₀	0.073 (0.016)	232.94 (0.59)	5.36 (1.53)	0.013	3.9
	C ¹⁸ O	2 – 1	0.231 (0.019)	234.85 (0.23)	6.17 (0.66)	0.035	4.8
N159S	H ₂ CO	3 ₀₃ – 2 ₀₂	0.056 (0.010)	235.87 (0.45)	4.45 (0.80)	0.012	3.9
	H ₂ CO	3 ₂₂ – 2 ₂₁	<0.005	4.9
	H ₂ CO	3 ₂₁ – 2 ₂₀	<0.005	3.4
	C ¹⁸ O	2 – 1	0.161 (0.006)	236.35 (0.07)	3.27 (0.19)	0.047	3.4
			0.047 (0.006)	232.39 (0.30)	3.40 (0.52)	0.013	3.4

Notes.

(a) Values in parenthesis are standard deviations from Gaussian fits using CLASS as part of the GILDAS software.

(b) Full width to half maximum line width.

3. Results

The three para-H₂CO lines are detected in all sources except N159S. There, only the strongest para-H₂CO line, the 3₀₃-2₀₂ transition, is detected. C¹⁸O (2-1), measured in 30 Dor, N159E, N159S, and N44BC, is detected in all sources. The para-H₂CO and C¹⁸O line spectra are presented in Figure 1. Line parameters are listed in Table 2, where velocity-integrated intensity, $\int T_{\text{mb}} dv$, local standard of rest velocity, V_{lsr} , full width to half maximum line width, FWHM, peak main beam brightness temperature, T_{mb} , and rms noise, were obtained from Gaussian fits.

3.1. Kinetic temperature and spatial density

To determine gas kinetic temperatures and spatial densities, we use the RADEX non-LTE model (van der Tak et al. 2007) of-fine code² with H₂CO collision rates from Wiesenfeld & Faure (2013) and C¹⁸O collision rates from Yang et al. (2010). The RADEX code needs five input parameters: background temperature, kinetic temperature, H₂ density, column density, and line width. For the background temperature, we adopt 2.73 K. Model grids for the para-H₂CO and C¹⁸O lines encompass 30 densities ($n(\text{H}_2) = 10^3 - 10^7 \text{ cm}^{-3}$) and 30 temperatures ranging from 10 to 110 K. For the line width, we use the observed line width value (Table 2). The total beam averaged column density of C¹⁸O can be obtained from the $J = 2-1$ integrated intensity following Batrla & Wilson (2003).

$$N(\text{C}^{18}\text{O}) = 5.3 \times 10^{14} \int T_{\text{mb}}(\text{C}^{18}\text{O}, J = 2 - 1) dv, \quad (1)$$

² <http://var.sron.nl/radex/radex.php>

where $\int T_{\text{mb}}(\text{C}^{18}\text{O}, J = 2 - 1) dv$ is the C¹⁸O (2-1) integrated intensity. The results are listed in Table 3. In the LMC, the gas is well mixed so that isotope ratios are pretty much the same throughout the galaxy (Johansson et al. 1994; Chin et al. 1997; Heikkilä et al. 1998, 1999; Wang et al. 2009). In the local ISM, the ¹⁶O/¹⁸O ratio is approximately 500 (Wilson & Rood 1994). We have, however, to keep in mind that fractional abundances in the LMC differ from those in the local ISM. In the LMC, ¹⁸O is underabundant with respect to ¹⁶O by about a factor of ~ 4 (¹⁶O/¹⁸O ~ 2000 in the LMC, Chin 1999; Wang et al. 2009), while ¹⁸O is underabundant by a factor of ~ 2.4 with respect to ¹⁷O (locally, ¹⁸O/¹⁷O ~ 4.1 , Zhang et al. 2007; Wouterloot et al. 2008; in the LMC ~ 1.7 , Heikkilä et al. 1998; Wang et al. 2009). Therefore, $N(\text{H}_2)/N(\text{C}^{18}\text{O})$ ratios should be higher by a factor of ~ 3 in the LMC with respect to the local ISM. This correlation will be used to derive H₂ column densities. The results for the H₂ column density are listed in Table 3. Assuming a CO to H₂ conversion factor of $X_{\text{CO}} \sim 4 \times 10^{20} \text{ cm}^{-2} (\text{K km s}^{-1})^{-1}$ for the LMC (Pineda et al. 2009; Wang et al. 2009), we can also derive a column density of $N(\text{H}_2)$ from the CO(1-0) integrated intensity moment map reported by Wong et al. (2011). The results of $N(\text{H}_2)$ are listed in Table 3. The H₂ column densities derived from C¹⁸O and CO are consistent with in the estimated uncertainty by a factor of two.

Previous observational results on transitions of C¹⁸O (1-0, 2-1) and para-H₂CO (2₀₂-1₀₁, 3₀₃-2₀₂, 3₂₂-2₂₁ and 3₂₁-2₂₀) using the 15 m Swedish-ESO Submillimetre Telescope (SEST) show that the column density ratio of $N(\text{C}^{18}\text{O})/N(\text{para-H}_2\text{CO})$ is ~ 100 in dense clumps of the LMC (Heikkilä et al. 1998, 1999; Wang et al. 2009). Assuming that the $N(\text{C}^{18}\text{O})/N(\text{para-H}_2\text{CO})$ ratio is the same in our sample, we estimate the column density

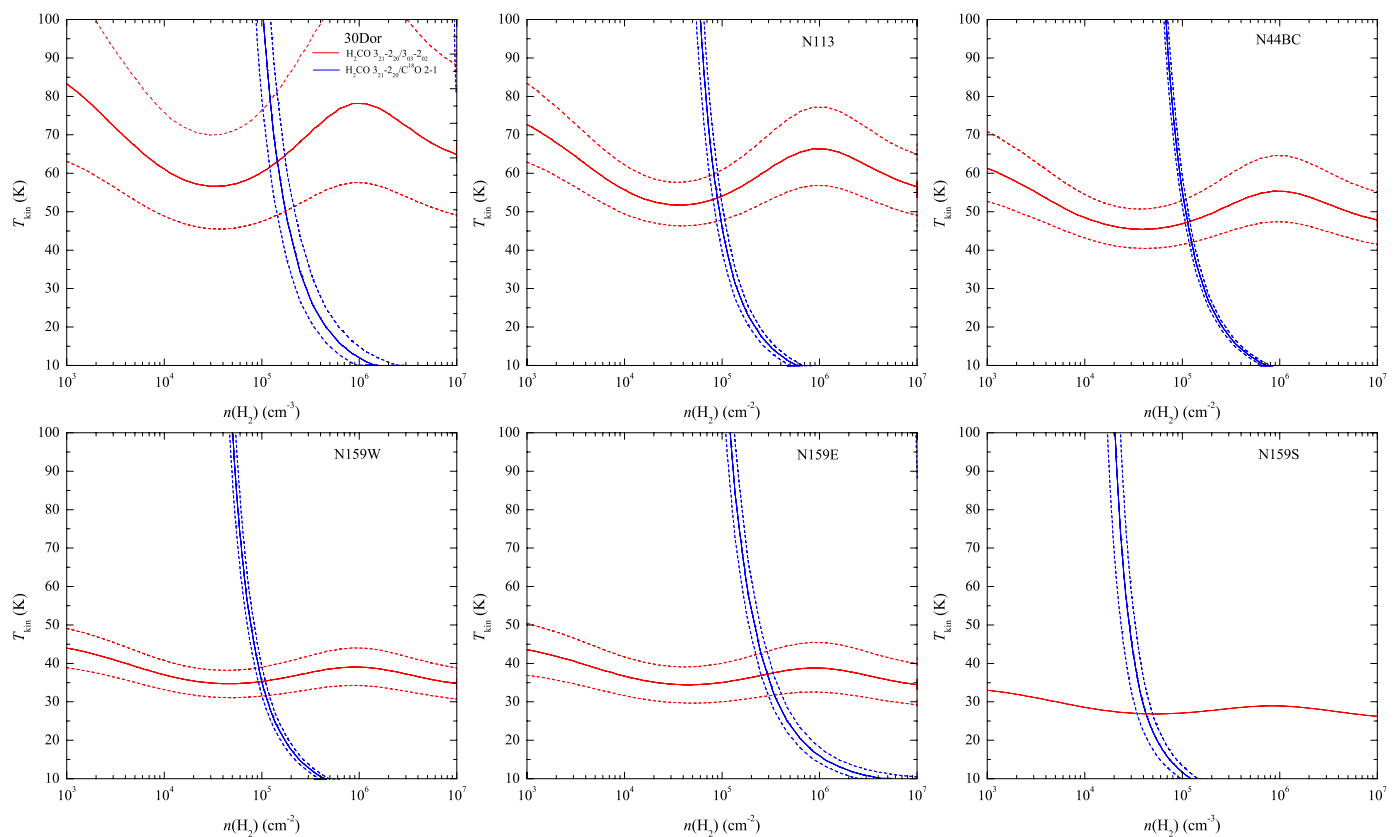


Fig. 2. RADEX non-LTE modeling of the gas kinetic temperature and spatial density, using the para-H₂CO 3₂₁-2₂₀/3₀₃-2₀₂ (red solid and dashed lines are observed values and uncertainties) and para-H₂CO 3₀₃-2₀₂/C¹⁸O 2-1 (blue solid and dashed lines) integrated intensity ratios. For details, see the notes to Table 3.

of para-H₂CO from the $N(\text{C}^{18}\text{O})$ column density. The results are listed in Table 3.

The para-H₂CO (3₀₃-2₀₂) line is the strongest of the three 218 GHz para-H₂CO transitions observed by us. In order to avoid small uncertain values in the denominator, the para-H₂CO 3₂₂-2₂₁/3₀₃-2₀₂ and 3₂₁-2₂₀/3₀₃-2₀₂ ratios are most suitable to derive the kinetic temperature. The para-H₂CO 3₂₂-2₂₁ and 3₂₁-2₂₀ transitions have similar energy above the ground state, $E_u \approx 68$ K, similar line brightness, and are often detected at the same time (e.g., Mühle et al. 2007; Bergman et al. 2011; Wang et al. 2012; Lindberg & Jørgensen 2012; Ao et al. 2013; Immer et al. 2014, 2016; Treviño-Morales et al. 2014; Ginsburg et al. 2016; Tang et al. 2016); therefore, para-H₂CO 3₂₂-2₂₁/3₀₃-2₀₂ and 3₂₁-2₂₀/3₀₃-2₀₂ ratios are both good thermometers to determine the gas temperature. The kinetic temperature is traced by these two ratios with an uncertainty of $\leq 25\%$ below 50 K (Mangum & Wootten 1993). While at $n(\text{H}_2) \gtrsim 10^5 \text{ cm}^{-3}$ both ratios are similarly suitable, the para-H₂CO 3₂₂-2₂₁/3₀₃-2₀₂ line ratio is affected by gas density at $n(\text{H}_2) < 10^5 \text{ cm}^{-3}$ (Tang et al. 2016). For our sample, spatial density measurements probed by molecular tracers like CS, SO, CO, CI, H₂CO, HCO⁺, and HCN (Heikkilä et al. 1998, 1999; Kim et al. 2004; Wang et al. 2009) show a range of $0.3 - 10 \times 10^5 \text{ cm}^{-3}$. Therefore, in this work we use the para-H₂CO 3₂₁-2₂₀/3₀₃-2₀₂ integrated intensity ratio to derive the kinetic temperature (Ginsburg et al. 2016; Immer et al. 2016).

In our Galaxy, spatial densities, $n(\text{H}_2)$, derived from para-H₂CO (3₀₃-2₀₂) are higher than from C¹⁸O (2-1). However, in the LMC, with lower density regions often being photoionized, this may be different. Therefore, here the para-H₂CO 3₀₃-2₀₂/C¹⁸O 2-

1 integrated intensity ratio is used to constrain the spatial density assuming the two tracers have a similar spatial extent and sample the same region. For both lines we find similar line parameters (e.g., V_{lsr} , FWHM, see Table 2) in our sample, so our assumption is reasonable. Figure 2 shows how the parameters are constrained by the line ratio distribution of para-H₂CO 3₂₁-2₂₀/3₀₃-2₀₂ and para-H₂CO 3₀₃-2₀₂/C¹⁸O 2-1 in the $T_{\text{kin}}-n(\text{H}_2)$ parameter space. The determined results are listed in Table 3. The spatial density of our sample derived from the para-H₂CO 3₀₃-2₀₂/C¹⁸O 2-1 ratio shows a relatively narrow range of $0.4 - 2.9 \times 10^5 \text{ cm}^{-3}$ with an average of $1.5 \pm 0.4 \times 10^5 \text{ cm}^{-3}$ (see Figure 2 and Table 3; errors given here and elsewhere are unweighted standard deviations of the mean), which is consistent with the results for the same dense clumps found from observations of e.g., SO, HCO⁺, c-C₃H₂, CH₃OH, and H₂CO (Heikkilä et al. 1999; Wang et al. 2009).

As already mentioned, our three para-H₂CO (3-2) transitions are sensitive to gas at density $\sim 10^5 \text{ cm}^{-3}$ (Immer et al. 2016). To highlight how much the derived kinetic temperature depends on the derived density based on the admittedly uncertain assumption that para-H₂CO 3₀₃-2₀₂ and C¹⁸O 2-1 trace the same gas, we have plotted in Figure 3 the relation between kinetic temperature and the para-H₂CO 3₂₁-2₂₀/3₀₃-2₀₂ ratio at spatial density $n(\text{H}_2) = 10^5 \text{ cm}^{-3}$ with column density of $N(\text{para-H}_2\text{CO}) = 2.1 \times 10^{12} \text{ cm}^{-2}$ and line width of 6 km s^{-1} (these are rough average values for our sample) using RADEX. Comparing this with the actually obtained values for individual sources derived from our para-H₂CO 3₂₁-2₂₀/3₀₃-2₀₂ and para-H₂CO 3₀₃-2₀₂/C¹⁸O 2-1 ratios, the plot demonstrates that the temperatures derived in the two different ways are in a good agreement.

Table 3. Integrated intensity ratios, column densities, spatial densities, and temperatures.

Sources	$3_{21-2_{20}}$	$\text{H}_2\text{CO } 3_{03-2_{02}}$	$N(\text{C}^{18}\text{O})$	$N(\text{para-H}_2\text{CO})$	$N(\text{H}_2)$		$n(\text{H}_2)$	T_{kin}	T_{LTE}	T_{dust}^c
	$3_{03-2_{02}}$	$\text{C}^{18}\text{O } 2-1$	$\times 10^{14} \text{ cm}^{-2}$	$\times 10^{12} \text{ cm}^{-2}$	C^{18}O	CO				
30 Dor	0.27±0.05	2.12±0.32	1.0	1.0	0.7	0.6	1.45 ^{+0.69} _{-0.42}	63.0 ^{+18.2} _{-13.9}	70.4	70–75
N113 ^a	0.23±0.03	1.22±0.12	2.7	2.7	2.0	1.0	0.89 ^{+0.18} _{-0.13}	53.6 ^{+6.7} _{-6.1}	54.1	30–51
N44BC	0.20±0.03	1.39±0.07	3.0	3.0	2.1	1.3	1.13 ^{+0.18} _{-0.16}	47.3 ^{+6.0} _{-5.4}	45.9	35–45
N159W ^b	0.13±0.02	1.01±0.08	3.7	3.7	2.7	1.8	1.00 ^{+0.20} _{-0.14}	35.3 ^{+3.7} _{-3.8}	32.0	30–40
N159E	0.13±0.03	2.39±0.21	1.2	1.2	0.9	0.8	2.92 ^{+1.15} _{-0.71}	37.2 ^{+5.9} _{-5.7}	46.4	30–40
N159S	<0.085	0.35±0.07	0.9	0.9	0.6	1.4	>0.43	<26.9	<25.1	20–30

Notes.

Column 4: Obtained from equation (1).

Column 5: Para-H₂CO column densities adopting $N(\text{C}^{18}\text{O})/N(\text{para-H}_2\text{CO}) = 100$ (see Section 3.1).

Column 6: H₂ column density derived from C¹⁸O with $X(\text{C}^{18}\text{O}/\text{H}_2) = 4.2 \times 10^{-8}$ (Frerking et al. 1982) and using the factor 3 correction explained in Section 3.1.

Column 7: H₂ column density obtained from ¹²CO(1-0) with a conversion factor of $X_{\text{CO}} = 4 \times 10^{20} \text{ cm}^{-2} (\text{K km s}^{-1})^{-1}$ (see Section 3.1).

Column 9: T_{kin} derived with the density given in column (8).

^aN113: Para-H₂CO $3_{03-2_{02}}/\text{C}^{18}\text{O } 2-1$ ratio data taken from Heikkilä et al. (1998) and Wang et al. (2009). $N(\text{C}^{18}\text{O})$ derived from C¹⁸O 2-1 taken from Heikkilä et al. (1998).

^bN159W: Para-H₂CO $3_{03-2_{02}}/\text{C}^{18}\text{O } 2-1$ ratio data taken from Heikkilä et al. (1998, 1999). $N(\text{C}^{18}\text{O})$ derived from C¹⁸O 2-1 taken from Heikkilä et al. (1998). $N(\text{H}_2)$ data taken from Ott et al. (2010).

^cDust temperature references:

30 Dor: Werner et al. (1978); Heikkilä et al. (1999); Gordon et al. (2014);

N113: Wang et al. (2009); Gordon et al. (2014); Seale et al. (2014);

N44BC: Gordon et al. (2014);

N159W: Heikkilä et al. (1999); Bolatto et al. (2000); Gordon et al. (2014);

N159E: Gordon et al. (2014);

N159S: Gordon et al. (2014).

The upper and lower limits in columns 2, 8, 9, and 10 correspond to 3σ values.

Local thermodynamic equilibrium (LTE) is a good approximation for the H₂CO level populations under optically thin high-density conditions (Mangum & Wootten 1993; Watanabe & Mitchell 2008). Although LTE and RADEX non-LTE models use different approximations and assumptions, it is useful to check how the temperatures derived by the two methods compare. The para-H₂CO line intensity ratios $3_{22-2_{21}}/3_{03-2_{02}}$ and $3_{21-2_{20}}/3_{03-2_{02}}$ can be used to measure the LTE kinetic temperature because (see Section 1) the $K_a = 0$ and 2 ladders of para-H₂CO are mainly connected by collisions. The LTE kinetic temperature can be calculated assuming that the lines are optically thin, and originate from a high-density region (Mangum & Wootten 1993).

$$T_{\text{kin}} = \frac{47.1}{\ln(0.556 \frac{I(3_{03-2_{02}})}{I(3_{22-2_{21}})})}, \quad (2)$$

where $I(3_{03-2_{02}})/I(3_{22-2_{21}})$ is the para-H₂CO integrated intensity ratio. The LTE kinetic temperatures are listed in Table 3. The uncertainty is $\lesssim 30\%$ for this method of temperature measurement (Mangum & Wootten 1993). Considering this uncertainty, the temperatures derived from LTE and the RADEX non-LTE model are consistent with each other.

3.2. Individual sources

Below, results from the six sources covered by this study are individually discussed.

3.2.1. 30 Dor

Our three para-H₂CO and C¹⁸O 2-1 transitions have already been observed toward 30 Dor by Heikkilä et al. (1999) with the SEST (beam size $\sim 23''$), but only para-H₂CO $3_{03-2_{02}}$ was detected.

With our higher sensitivity we detect all four lines and confirm their para-H₂CO results. The kinetic temperature derived from para-H₂CO ($3_{21-2_{20}}/3_{03-2_{02}}$) is ~ 63 K, which is the highest value determined in our sample. 30 Dor, hosting a cluster of O3 stars that rivals super star clusters, is the most spectacular star forming region in the Local Group (Walborn & Blades 1997; Massey & Hunter 1998), which makes such a high T_{kin} value comprehensible. The spatial density derived from the para-H₂CO $3_{03-2_{02}}/\text{C}^{18}\text{O } 2-1$ ratio is $\sim 1.5 \times 10^5 \text{ cm}^{-3}$ at this temperature, which agrees with results derived from other species (e.g., CS, SO, HCO⁺, Heikkilä et al. 1999).

3.2.2. N113

All three 218 GHz para-H₂CO lines as well as C¹⁸O 2-1 transition have been observed by Wang et al. (2009) and Heikkilä et al. (1998) with the SEST. Para-H₂CO $3_{03-2_{02}}$ and C¹⁸O 2-1 were detected. We detect the three transitions of para-H₂CO for the first time. The kinetic temperature derived from para-H₂CO ($3_{21-2_{20}}/3_{03-2_{02}}$) is ~ 54 K. N113 is the LMC star forming region with the most luminous 22 GHz H₂O maser (Whiteoak & Gardner 1986; Lazendic et al. 2002; Oliveira et al. 2006), not quite as spectacular as 30 Dor, but hosts a few bright HII regions whose stellar energy feedback is likely to have elevated its temperature, thus leading to the second highest T_{kin} value. The spatial density derived from para-H₂CO $3_{03-2_{02}}/\text{C}^{18}\text{O } 2-1$ (ratio data from Wang et al. (2009) and Heikkilä et al. (1998), assuming that the para-H₂CO $3_{03-2_{02}}/\text{C}^{18}\text{O } 2-1$ ratio at the SEST beam size, $\sim 23''$, is similar to that in the APEX beam size, $\sim 30''$, see Section 3.2.4) is $\sim 8.9 \times 10^4 \text{ cm}^{-3}$ at temperature ~ 54 K, which agrees with results from other molecules (e.g., CS, HCO⁺, HCN, Wang et al. 2009).

3.2.3. N44BC

C¹⁸O 2-1 has been detected in N44BC by Heikkilä et al. (1998) with the SEST. We detect the three 218 GHz para-H₂CO transitions and the C¹⁸O line. Our observations confirm their C¹⁸O 2-1 result. The kinetic temperature derived by para-H₂CO ($3_{21-2_{20}}/3_{03-2_{02}}$) is ~ 47 K. Such a high temperature likely results from the stellar energy feedback from the adjacent super bubble on the molecular cloud, which also shows bright mid-IR emission (Chen et al. 2009). The spatial density derived from the para-H₂CO $3_{03-2_{02}}/C^{18}O$ 2-1 ratio is $\sim 1.1 \times 10^5$ cm⁻³ at this temperature, which agrees with results from other molecules (e.g., CO, CI, Heikkilä et al. 1998; Kim et al. 2004).

3.2.4. N159W

The three para-H₂CO 218 GHz transitions as well as C¹⁸O 2-1 have been detected in N159W by Heikkilä et al. (1998, 1999) with the SEST. Our observations confirm their para-H₂CO results. The kinetic temperature derived by para-H₂CO ($3_{21-2_{20}}/3_{03-2_{02}}$) is ~ 35 K. The spatial density derived from the para-H₂CO $3_{03-2_{02}}/C^{18}O$ 2-1 ratio (data from Heikkilä et al. 1998, 1999) is $\sim 1.0 \times 10^5$ cm⁻³ at this temperature, which agrees with results measured by other species (e.g., CS, SO, Heikkilä et al. 1999). To quantify potential differences in temperature and density derived from APEX and SEST data, we determined the temperature and the density with the same method using the SEST para-H₂CO and C¹⁸O data from Heikkilä et al. (1998, 1999). The derived temperature and density are $30.3^{+5.7}_{-5.4}$ K and $1.14^{+0.35}_{-0.23} \times 10^5$ cm⁻³, respectively. This indicates nearly the same spatial density and a few Kelvin difference for the kinetic temperature. This temperature difference is similar to its 1σ uncertainty (~ 6 K). Therefore, the temperature gradient and density gradient is small when moving from a beam size of 7.3 pc (APEX) to 5.6 pc (SEST).

3.2.5. N159E

The three para-H₂CO 218 GHz transitions as well as C¹⁸O 2-1 are detected. To our knowledge, it is the first detection of para-H₂CO in the N159E region. The source shows similar properties as N159W. The kinetic temperature derived from para-H₂CO ($3_{21-2_{20}}/3_{03-2_{02}}$) is ~ 37 K. The spatial density derived from the para-H₂CO $3_{03-2_{02}}/C^{18}O$ 2-1 ratio is $\sim 2.9 \times 10^5$ cm⁻³ at this temperature.

3.2.6. N159S

Two velocity components are detected by C¹⁸O, at 232.4 and 236.4 km s⁻¹. Para-H₂CO $3_{03-2_{02}}$ is detected at a velocity of 235.9 km s⁻¹ (see Table 2). However, the para-H₂CO $3_{22-2_{21}}$ and $3_{21-2_{20}}$ lines are not detected. The dust temperature ranges from 20 to 30 K (Gordon et al. 2014). N159S appears to be a cold cloud (Heikkilä et al. 1999), and has been shown to host no massive star formation at present and during the last 10 Myr (Chen et al. 2010). The upper limit to the kinetic temperature derived from para-H₂CO ($3_{21-2_{20}}/3_{03-2_{02}}$) based on our observational 3σ limit for the $3_{21-2_{20}}$ line is ~ 27 K. The spatial density derived from the para-H₂CO $3_{03-2_{02}}/C^{18}O$ 2-1 ratio is $>4.3 \times 10^4$ cm⁻³, which is consistent with results measured by other species (e.g., CS, SO, Heikkilä et al. 1999).

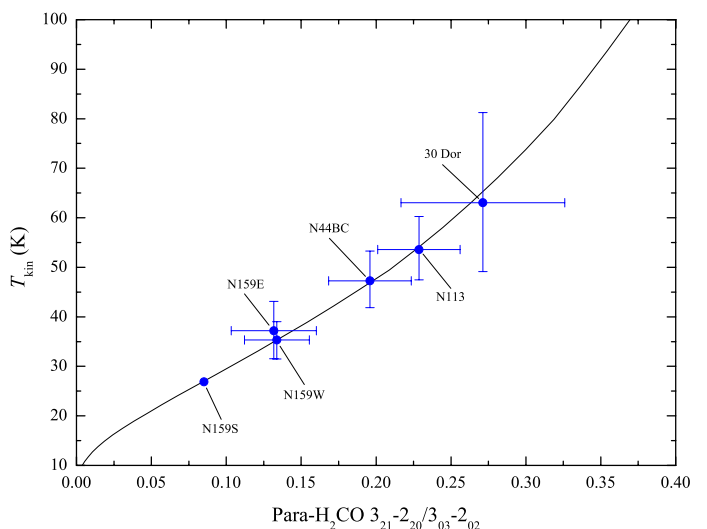


Fig. 3. RADEX non-LTE modeling of the relation between the gas kinetic temperature and the para-H₂CO $3_{21-2_{20}}/3_{03-2_{02}}$ integrated intensity ratio (solid line), assuming $n(\text{H}_2) = 10^5$ cm⁻³, $N(\text{para-H}_2\text{CO}) = 2.1 \times 10^{12}$ cm⁻², and a line width of 6 km s⁻¹. Blue points are the results derived from the measured para-H₂CO $3_{21-2_{20}}/3_{03-2_{02}}$ and para-H₂CO $3_{03-2_{02}}/C^{18}O$ 2-1 ratios. For N159S, 3σ upper limits for the line ratio and the kinetic temperature have been taken.

4. Discussion

4.1. Comparison of temperatures derived from H₂CO, CO, NH₃, and the dust

The kinetic temperatures of molecular clumps in the LMC have been calculated by multi-transition data of CO (Johansson et al. 1998; Heikkilä et al. 1999; Israel et al. 2003; Kim et al. 2004; Bolatto et al. 2005; Pineda et al. 2008; Mizuno et al. 2010; Minamidani et al. 2008, 2011; Fujii et al. 2014; Paron et al. 2016). These observations show that the higher temperatures ($T_{\text{kin}} \geq 100$ K) occur in cloud regions that are of lower density ($\lesssim 10^3$ cm⁻³) and that the gas is colder ($T_{\text{kin}} = 10 - 80$ K) in regions of higher density ($10^4 - 10^5$ cm⁻³). As already mentioned in Section 3.1, the spatial density range of our sample derived from the para-H₂CO $3_{03-2_{02}}/C^{18}O$ 2-1 ratio with respect to the Galaxy is $0.4 - 2.9 \times 10^5$ cm⁻³ with an average of $1.5 \pm 0.4 \times 10^5$ cm⁻³. Excluding the quiescent cloud N159S, where only one para-H₂CO line could be detected, the gas kinetic temperatures derived from para-H₂CO ($3_{21-2_{20}}/3_{03-2_{02}}$), range from 35 to 63 K with an average of 47 ± 5 K. Temperatures and densities derived from CO are for 30 Dor $T_{\text{kin}} \sim 40 - 80$ K and $n(\text{H}_2) \sim 3 \times 10^3 - 3 \times 10^5$ cm⁻³ (Johansson et al. 1998; Heikkilä et al. 1999; Minamidani et al. 2008), N159W $T_{\text{kin}} \sim 16 - >30$ K and $n(\text{H}_2) \sim 3 \times 10^3 - 8 \times 10^5$ cm⁻³ (Johansson et al. 1998; Heikkilä et al. 1999; Bolatto et al. 2005; Minamidani et al. 2008), N159E $T_{\text{kin}} > 40$ K and $n(\text{H}_2) \sim 1 \times 10^3 - 3 \times 10^5$ cm⁻³ (Minamidani et al. 2008), and N159S $T_{\text{kin}} \sim 10 - 60$ K and $n(\text{H}_2) \sim 1 \times 10^3 - 1 \times 10^5$ cm⁻³ (Heikkilä et al. 1999; Minamidani et al. 2008). Temperatures derived from para-H₂CO are consistent with but much more precise than the results derived from CO in the dense regions ($>10^3$ cm⁻³).

Except for N159E, all our sources have been surveyed in NH₃ (1,1) and (2,2) by Ott et al. (2010). These lines are only detected in the massive star-forming region N159W. We compare fractional abundances of $N(\text{para-NH}_3)/N(\text{H}_2)$ and $N(\text{para-H}_2\text{CO})/N(\text{H}_2)$ to column density $N(\text{H}_2)$ obtained from ¹²CO(1-

0) in Figure 4. These show that formaldehyde has a stable fractional abundance ranging from 0.6 to $5.7 \times 10^{-10} \text{ cm}^{-2}$ with an average of $2.7 \pm 1.8 \times 10^{-10} \text{ cm}^{-2}$ in molecular clouds of the LMC with $N(\text{H}_2)$ column densities ranging from 0.4 to $2 \times 10^{22} \text{ cm}^{-2}$. Ammonia only survives in a high column density environment with $N(\text{H}_2) \sim 2 \times 10^{22} \text{ cm}^{-2}$. The fractional abundance of ammonia is $\sim 10^{-10} - 10^{-9}$ in N159W and M82, which is similar to that of formaldehyde in the LMC. As already mentioned, the kinetic temperature derived from the $\text{NH}_3(2,2)/(1,1)$ line ratio in N159W is $\sim 16 \text{ K}$ (Ott et al. 2010), which is two times lower than that derived from para- H_2CO . Previous para- $\text{H}_2\text{CO}(3_{22}-2_{21}/3_{03}-2_{02})$ and $\text{NH}_3(2,2)/(1,1)$ observations toward the starburst galaxy M82 also show significantly different gas kinetic temperatures (Weiß et al. 2001; Mühle et al. 2007). M82, a satellite galaxy like the LMC, shows a similar environment, involving low metallicity combined with a high UV flux. This only leaves NH_3 surviving in the most shielded pockets of molecular gas, resulting in a low fractional abundance (see Figure 4) and a low kinetic temperature. Furthermore, this abundance is demonstrating in an exemplary way that H_2CO is less affected by photodissociation, sampling a more extended region. Therefore, para- H_2CO traces in these instances a higher temperature than $\text{NH}_3(2,2)/(1,1)$. We conclude that para- H_2CO line ratios are a superior thermometer to trace dense gas temperatures in low metallicity galaxies with strong UV radiation. Nevertheless, more detailed spatially resolved comparisons of H_2CO with NH_3 temperatures would be very interesting because it could provide more information on temperature gradients and the location of different kinetic temperature layers.

The temperatures derived from dust and gas are often in agreement in the active and dense clumps of Galactic disk clouds (Dunham et al. 2010; Giannetti et al. 2013; Battersby et al. 2014). However, observed gas and dust temperatures do not agree with each other in the Galactic Central Molecular Zone (CMZ) and external galaxies (Güsten et al. 1981; Ao et al. 2013; Mangum et al. 2013a; Ott et al. 2014; Ginsburg et al. 2016; Immer et al. 2016). Dust temperatures in the LMC have been obtained by Gordon et al. (2014) using Herschel 100 to 500 μm dust continuum emission data. They range approximately from 13 to 73 K. For our sample, the dust temperatures range from 30 to 75 K (Werner et al. 1978; Heikkilä et al. 1999; Bolatto et al. 2000; Wang et al. 2009; Seale et al. 2014; Gordon et al. 2014) while the para- H_2CO derived temperature ranges from 35 to 63 K. The temperatures derived from para- H_2CO ratios and dust emission are therefore in good agreement (see Table 3). This indicates that the dust and H_2CO kinetic temperatures are equivalent in the star forming regions of the LMC. Assuming that H_2CO traces the bulk of the dense molecular gas and that ammonia shows very low abundances, this can be generalized in the sense that dense gas and dust temperatures are generally equivalent.

4.2. Star-forming regions in the Galaxy, the LMC, and other galaxies

The gas temperatures of ATLASGAL (APEX Telescope Large Area Survey of the GALaxy) massive star forming clumps have been measured by para- $\text{H}_2\text{CO}(3_{03}-2_{02}, 3_{22}-2_{21}, \text{ and } 3_{21}-2_{20})$ line ratios (Tang et al. 2016). The thus derived gas kinetic temperatures at density $n(\text{H}_2) = 10^5 \text{ cm}^{-3}$ with size of $0.3 - 0.7 \text{ pc}$ range from 30 to 61 K with an average of $46 \pm 9 \text{ K}$, which agrees remarkably well with the results in the LMC with a beam size of $\sim 7 \text{ pc}$. Large area mapping measurements of kinetic temperatures in the Galactic CMZ with the same transitions of para-

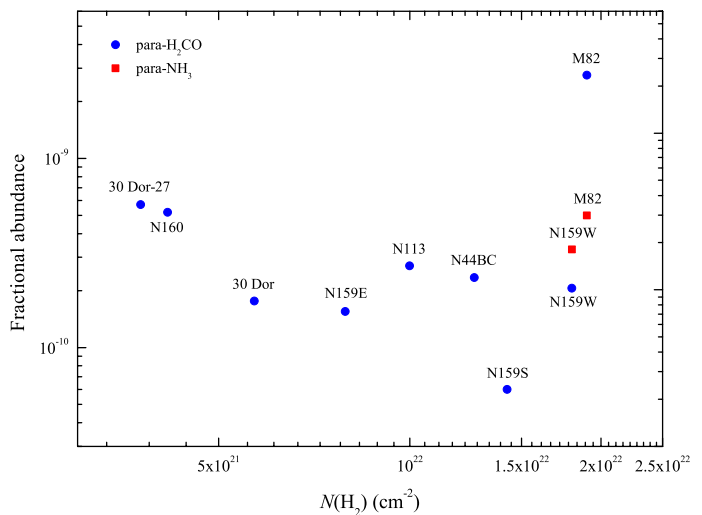


Fig. 4. Abundances of $N(\text{para-NH}_3)/N(\text{H}_2)$, red squares, and $N(\text{para-H}_2\text{CO})/N(\text{H}_2)$, blue points, vs. column density $N(\text{H}_2)$ obtained from ^{12}CO . 30 Dor-27 and N160 data taken from Heikkilä et al. (1999). N159W data taken from Ott et al. (2010). M82 data taken from Weiß et al. (2001) and Mühle et al. (2007).

H_2CO (Ao et al. 2013; Ginsburg et al. 2016) suggest that the mean gas temperature is $\sim 48 \text{ K}$ at $n(\text{H}_2) = 10^5 \text{ cm}^{-3}$ or $\sim 65 \text{ K}$ at $n(\text{H}_2) = 10^4 \text{ cm}^{-3}$ in the whole $\sim 300 \text{ pc}$ surveyed region. It shows a higher T_{kin} value than our observed results. The spatial densities derived from the para- $\text{H}_2\text{CO} 3_{03}-2_{02}/\text{C}^{18}\text{O} 2-1$ ratio in our sample agree with the observed results in the Galactic clumps (Beuther et al. 2002; Motte et al. 2003; Wienen et al. 2012, 2015), HII regions (Henkel et al. 1983; Ginsburg et al. 2011), and giant molecular clouds (GMCs) (Wadiak et al. 1988; Ginsburg et al. 2015; Immer et al. 2016). This agreement indicates that the physical conditions of the star forming regions should be similar in both the LMC and our Galactic disk.

Using the three transitions of para- H_2CO at $\sim 218 \text{ GHz}$ to measure the kinetic temperature of the starburst galaxy M82 shows that the derived kinetic temperature ($T_{\text{kin}}(\text{H}_2\text{CO}) \sim 200 \text{ K}$; Mühle et al. 2007) is significantly higher than in the LMC. Kinetic temperatures of starburst galaxies measured with multi-inversion transitions of NH_3 show a range from 24 to $\geq 250 \text{ K}$ (Henkel et al. 2000, 2008; Mauersberger et al. 2003; Ao et al. 2011; Lebrón et al. 2011; Mangum et al. 2013a). The temperatures derived from para- H_2CO line ratios in the LMC overlap with the values found for a sample at lower temperature (e.g., M83, NGC6946). This is likely due to the inclusion of higher excited ammonia lines, which, however, should be difficult to detect in the LMC because there particularly warm regions irradiated by enhanced UV radiation should be almost devoid of NH_3 . The spatial densities in starburst galaxies derived from ortho- $\text{H}_2\text{CO}(2_{11}-2_{12}/1_{10}-1_{11})$ line ratios (Mangum et al. 2008, 2013b) show a similar range ($10^{4.5}-10^{5.5} \text{ cm}^{-3}$) to that derived from para- $\text{H}_2\text{CO} 3_{03}-2_{02}/\text{C}^{18}\text{O} 2-1$ ratios in the LMC. This indicates that star formation in the LMC and external galaxies may arise from dense molecular gas ($>10^4 \text{ cm}^{-3}$), but gas heating rates may be quite different.

4.3. Correlation of gas temperature with star formation

In star forming galaxies, a lack of correlation between the gas kinetic temperatures traced by NH_3 and star formation rate in-

indicated by infrared luminosity was found by Mangum et al. (2013a). To investigate how the kinetic temperatures traced by para-H₂CO correlate with star formation in the LMC, we compared the gas kinetic temperature to the Herschel 250 μ m dust emission which indicates the infrared luminosity (Seale et al. 2014). We averaged the Herschel 250 μ m data over a 30'' beam corresponding to our para-H₂CO data. A comparison between gas kinetic temperatures derived from para-H₂CO and the Herschel 250 μ m flux is shown in Figure 5. It reveals a correlation of gas temperature and 250 μ m flux for the five sources with all 218 GHz para-H₂CO lines detected (slope = 0.97 ± 0.49 , correlation coefficient $R \sim 0.75$). According to the relation between the infrared luminosity and 250 μ m flux $L_{\text{FIR}} \propto F_{250}^{1.2}$ in the LMC (Seale et al. 2014), the infrared luminosity and the gas temperature derived from para-H₂CO are related by a power-law of the form $L_{\text{FIR}} \propto T_{\text{kin}}^{1.2 \pm 0.59}$ where the power-law index is lower than that of the Stefan-Boltzmann law ($L \propto T_{\text{kin}}^4$). This suggests that this picture is an oversimplification, and that star formation occurs in extended regions leading to the formation of stellar clusters with multiple FIR sources (e.g., Chen et al. 2009, 2010). Assuming that the 250 μ m flux is mostly coming from clusters of FIR sources distributed across the regions from where the H₂CO emission is arising, this can be generalized in the sense that the gas heating mechanism must be related to the formation of young massive stars. To find out whether the bulk of the H₂CO emission is originating from within individual clusters of FIR sources, in between adjacent such FIR clusters, or both, higher resolution H₂CO observations would be mandatory.

We need more data points in the LMC to understand the relationship between T_{kin} and star formation and to then apply this relationship to more distant galaxies with ALMA. Para-H₂CO 3₂₁₋₂₂₀/3₀₃₋₂₀₂ and para-H₂CO 3₀₃₋₂₀₂/C¹⁸O 2-1 line ratios provide a direct estimate of the gas kinetic temperatures and spatial densities for molecular gas on a scale of ~ 7 pc in the star forming regions of the LMC. It would be meaningful to use these line ratios to measure the physical properties of the dense molecular gas at smaller linear scales with ALMA and to start systematic investigations in more distant star-forming galaxies.

5. Summary

We have measured the kinetic temperature and spatial density with para-H₂CO ($J_{K_A K_C} = 3_{03-202}$, 3_{22-221} , and 3_{21-220}) line ratios and the C¹⁸O 2-1 line in massive star-forming regions of the LMC. Kinetic temperatures derived from the above mentioned formaldehyde 218 GHz line triplet are compared with those obtained from the dust and, in one case, also from ammonia using the 12-m APEX telescope. The main results are the following:

1. Using the RADEX non-LTE program, we derive gas kinetic temperatures and spatial densities modeling the measured para-H₂CO 3₂₁₋₂₂₀/3₀₃₋₂₀₂ and para-H₂CO 3₀₃₋₂₀₂/C¹⁸O 2-1 line ratios.
2. The gas kinetic temperatures derived from para-H₂CO (3₂₁₋₂₂₀/3₀₃₋₂₀₂) line ratios of the star forming regions in the LMC are warm, ranging from 35 to 63 K with an average of 47 ± 5 K, which is similar to that obtained from Galactic disk massive star forming clumps.
3. The spatial density derived from the para-H₂CO 3₀₃₋₂₀₂/C¹⁸O 2-1 ratio shows a range of $0.4 - 2.9 \times 10^5 \text{ cm}^{-3}$ with an average of $1.5 \pm 0.4 \times 10^5 \text{ cm}^{-3}$. It agrees with results measured by ortho-H₂CO (2₁₁₋₂₁₂/1₁₀₋₁₁₁) line ratios in Galactic regions of massive star formation.

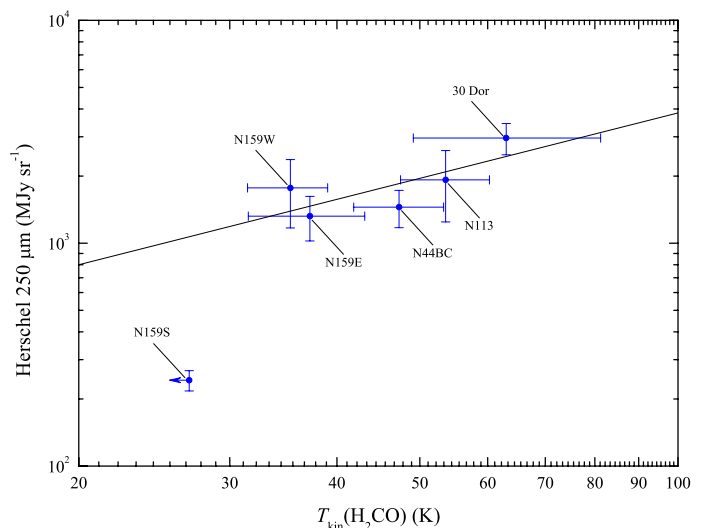


Fig. 5. Comparison of gas kinetic temperatures derived from para-H₂CO 3₂₁₋₂₂₀/3₀₃₋₂₀₂ against the Herschel 250 μ m flux. The straight line is the result from a linear fit for the five sources with all 218 GHz para-H₂CO lines detected. N159S provides with respect to T_{kin} a 3σ upper limit. Thus this point may actually be located much further to the left, closer to the linear fit obtained from the other five sources.

4. Temperatures derived from the para-H₂CO line ratios agree with those derived from CO in dense regions ($n(\text{H}_2) > 10^3 \text{ cm}^{-3}$). The gas temperature derived from the NH₃ (2,2)/(1,1) line ratio is ~ 16 K in N159W (Ott et al. 2010), which is two times lower than the temperature derived from the para-H₂CO line ratio and the dust. Ammonia only survives in the most shielded pockets of molecular gas in the LMC's low metallicity environment affected by a high UV flux. Formaldehyde is less affected by photodissociation and traces a more extended region.
5. A comparison of the gas kinetic temperature derived from para-H₂CO and the temperature obtained from dust emission shows good agreement. It indicates that the bulk of the dense gas and dust are in approximate thermal equilibrium in the dense star formation regions of the LMC.
6. A correlation between the gas kinetic temperatures derived from para-H₂CO and infrared luminosity indicated by the 250 μ m flux suggests that our kinetic temperatures traced by para-H₂CO are closely associated with extended star formation in the LMC.

Acknowledgements. We thank the staff of the APEX telescope for their assistance in observations. The authors are also thankful for the helpful comments of the anonymous referee. This work was funded by The National Natural Science Foundation of China under grant 11433008 and The Program of the Light in China's Western Region (LCRW) under grant Nos.XBBS201424 and The National Natural Science Foundation of China under grant 11373062. C.H acknowledges support by a visiting professorship for senior international scientists of the Chinese Academy of Sciences (2013T2J0057). This research has used NASA's Astrophysical Data System (ADS).

References

- Ao, Y., Henkel, C., Menten, K. M., et al. 2013, A&A, 550, 135
 Ao, Y., Henkel, C., Braatz, J. A., et al. 2011, A&A, 529, 154
 Baan, W. A., Güsten, R., & Haschick, A. D. 1986, ApJ, 305, 830
 Baan, W. A., Haschick, A. D., & Uglesich, R. 1993, ApJ, 415, 140
 Baan, W. A., Henkel, C., Schilke, P., et al. 1990, ApJ, 353, 132
 Batrla, W. & Wilson, T. L. 2003, A&A, 408, 231

- Battersby, C., Bally, J., Dunham, M., et al. 2014, *ApJ*, 786, 116
- Benson, P. J., & Myers, P. C. 1983, *ApJ*, 270, 589
- Bergman, P., Parise, B., Liseau, R., & Larsson, B. 2011, *A&A*, 527, 39
- Beuther, H., Schilke, P., Menten, K. M., et al. 2002, *ApJ*, 566, 945
- Bieging, J. H., Wilson, T. L., & Downes, D. 1982, *A&AS*, 49, 607
- Bolatto, A. D., Israel, F. P., & Martin, C. L. 2005, *ApJ*, 633, 210
- Bolatto, A. D., Jackson, J. M., Israel, F. P., et al. 2000, *ApJ*, 545, 234
- Caselli, P., Hasegawa, T. I., & Herbst, E. 1993, *ApJ*, 408, 548
- Chen, C.-H. R., Chu, Y. H., Gruendl, R. A. et al. 2009, *ApJ*, 695, 511
- Chen, C.-H. R., Indebetouw, R., Chu, Y. H. et al. 2010, *ApJ*, 721, 1206
- Chin, Y. 1999, *IAUS*, 190, 279
- Chin, Y. N., Henkel, C., Whiteoak, J. B. et al. 1997, *A&A*, 317, 548
- Chira, R. A., Beuther, H., Linz, H., et al. 2013, *A&A*, 552, 40
- Cohen, R. J., & Few, R. W. 1981, *MNRAS*, 194, 711
- Cohen, R. J., Matthews, N., Few, R. W., et al. 1983, *MNRAS*, 203, 1123
- Danby, G., Flower, D. R., Valiron, P., et al. 1988, *MNRAS*, 235, 229
- Downes, D., Wilson, T. L., Bieging, J., & Wink, J. 1980, *A&AS*, 40, 379
- Dunham, M. K., Rosolowsky, E., Evans, N. J. II., et al. 2010, *ApJ*, 717, 1157
- Fujii, K., Minamidani, T., Mizuno, N., Onishi, T., et al. 2014, *ApJ*, 796, 123
- Frerking, M. A., Langer, W. D., & Wilson, R. W. 1982, *ApJ*, 262, 590
- Giannetti, A., Brand, J., Sánchez-Monge, Á., et al. 2013, *A&A*, 556, 16
- Ginsburg, A., Bally, J., Battersby, C., et al. 2015, *A&A*, 573, 106
- Ginsburg, A., Darling, J., Battersby, C., et al. 2011, *ApJ*, 736, 149
- Ginsburg, A., Henkel, C., Ao, Y., et al. 2016, *A&A*, 586, 50
- Gordon, K. D., Roman-Duval, J., Bot, C., et al. 2014, *ApJ*, 797, 85
- Guo, W. H., Esimbek, J., Tang, X. D., et al. 2016, *Ap&SS*, 361, 264
- Güsten, R. & Henkel, C. 1983, *A&A*, 125, 136
- Güsten, R., Walmsley, C. M., & Pauls, T. 1981, *A&A*, 103, 197
- Heikkilä, A., Johansson, L. E. B., & Olofsson, H. 1998, *A&A*, 332, 493
- Heikkilä, A., Johansson, L. E. B., & Olofsson, H. 1999, *A&A*, 344, 817
- Henkel, C., Baan, W. A., & Mauersberger, R. 1991, *A&ARv*, 3, 47
- Henkel, C., Braatz, J. A., Menten, K. M., & Ott, J. 2008, *A&A*, 485, 451
- Henkel, C., Mauersberger, R., Peck, A. B., et al. 2000, *A&A*, 361L, 45
- Henkel, C., Wilson, T. L., Walmsley, C. M., & Pauls, T. 1983, *A&A*, 127, 388
- Hidaka, H., Watanabe, N., Shiraki, T., et al. 2004, *ApJ*, 614, 1124
- Ho P. T. P., & Townes, C. H., 1983, *ARA&A*, 21, 239
- Hüttemeister, S., Mauersberger, R., & Henkel, C., 1997, *A&A*, 326, 59
- Immer, K., Galván-Madrid, R., König, C., et al. 2014, *A&A*, 572, 63
- Immer, K., Kauffmann, J., Pillai, T., et al. 2016, *A&A*, 595, 94
- Israel, F. P., Johansson, L. E. B., Rubio, M., et al. 2003, *A&A*, 406, 817
- Johansson, L. E. B., Greve, A., Booth, R. S., et al. 1998, *A&A*, 331, 857
- Johansson, L. E. B., Olofsson, H., Hjalmarsen, A., et al. 1994, *A&A*, 291, 89
- Johnstone, D., Boonman, A. M. S. & van Dishoeck, E. F. 2003, *A&A*, 412, 157
- Johnston, K. G., Beuther, H., Linz, H., et al. 2014, *A&A*, 568, 56
- Kim, S., Walsh, W., & Xiao, K. 2004, *ApJ*, 616, 865
- Lazendic, J. S., Whiteoak, J. B., Klamer, I., et al. 2002, *MNRAS*, 331, 969
- Lebrón, M., Mangum, J. G., Mauersberger, R. et al. 2011, *A&A*, 534, 56
- Lindberg, J. E., & Jørgensen, J. K. 2012, *A&A*, 548, 24
- Mangum, J. G., Darling, J., Henkel, C., et al. 2013a, *ApJ*, 779, 33
- Mangum, J. G., Darling, J., Henkel, C., & Menten, K. M. 2013b, *ApJ*, 766, 108
- Mangum, J. G., Darling, J., Menten, K. M., & Henkel, C. 2008, *ApJ*, 673, 832
- Mangum, J. G., & Wootten, A. 1993, *ApJS*, 89, 123
- Mangum, J. G., Wootten, A., & Plambeck, R. L. 1993, *ApJ*, 409, 282
- Mangum, J. G., Wootten, A., Wadiak, E. J., & Loren, R. B. 1990, *ApJ*, 348, 542
- Massey, P., & Hunter, D. A. 1998, *ApJ*, 493, 180
- Mauersberger, R., Henkel, C., Weiß, A., et al. 2003, *A&A*, 403, 561
- Mauersberger, R., Henkel, C., & Wilson, T. L. 1987, *A&A*, 173, 352
- Minamidani, T., Mizuno, N., Mizuno, Y., et al. 2008, *ApJS*, 175, 485
- Minamidani, T., Tanaka, T., Mizuno, Y., et al. 2011, *AJ*, 141, 73
- Mitchell, G. F., Johnstone, D., Moriarty-Schieven, G., et al. 2001, *ApJ*, 556, 215
- Mizuno, Y., Kawamura, A., Onishi, T., et al. 2010, *PASJ*, 62, 51
- Motte, F., Schilke, P., & Lis, D. C. 2003, *ApJ*, 582, 277
- Mühle, S., Seaquist, E. R., & Henkel, C. 2007, *ApJ*, 671, 1579
- Oliveira, J. M., van Loon, J. Th., Stanimirović, S., & Zijlstra, A. A. 2006, *MNRAS*, 372, 1509
- Ott, J., Henkel, C., Braatz, J. A., & Weiß, A. 2011, *ApJ*, 742, 95
- Ott, J., Henkel, C., Staveley-Smith, L., & Weiß, A. 2010, *ApJ*, 710, 105
- Ott, J., Weiß, A., Staveley-Smith, L., et al. 2014, *ApJ*, 785, 16
- Paron, S., Ortega, M. E., Fariña, C., et al. 2016, *MNRAS*, 455, 518
- Pineda, J. L., Mizuno, N., Stutzki, J., et al. 2008, *A&A*, 482, 197
- Pineda, J. L., Ott, J., Klein, U., et al. 2009, *ApJ*, 703, 736
- Pietrzyński, G., Graczyk, D., Gieren, W., et al. 2013, *Natur*, 495, 76
- Qin, S. L., Zhao, J. H., Moran, J. M., et al. 2008, *ApJ*, 677, 353
- Rolleston, W. R. J., Trundle, C., & Dufton, P. L. 2002, *A&A*, 396, 53
- Seale, J. P., Meixner, M., Sewiło, M., et al. 2014, *AJ*, 148, 124
- van der Tak, F. F. S., Black, J. H., Schier, F. L., et al. 2007, *A&A*, 468, 627
- Tang, X. D., Esimbek, J., Zhou, J. J., et al. 2013, *A&A*, 551, 28
- Tang, X. D., Henkel, C., Menten, K. M., et al. 2016, *arXiv*, 1610, 05548
- Treviño-Morales, S. P., Pilleri, P., Fuente, A., et al. 2014, *A&A*, 569, 19
- Wadiak, E. J., Rood, R. T., & Wilson, T. L. 1988, *ApJ*, 324, 931
- Walborn, N. R., & Blades, J. C. 1997, *ApJS*, 112, 457
- Walmsley, C. M., & Ungerechts, H. 1983, *A&A*, 122, 164
- Wang, M., Chin, Y.-N., Henkel, C., et al. 2009, *ApJ*, 690, 580
- Wang, M., Henkel, C., Chin, Y.-N., et al. 2004, *A&A*, 422, 883
- Wang, Y., Beuther, H., Zhang, Q., et al. 2012, *ApJ*, 754, 87
- Watanabe, N., & Kouchi, A. 2002, *ApJ*, 571, 173
- Watanabe, T., & Mitchell, G. 2008, *AJ*, 136, 1947
- Weiß, A., Neininger, N., Henkel, C., Stutzki, J., & Klein, U. 2001, *ApJ*, 554, 143
- Werner, M. W., Becklin, E. E., Gatley, I., et al., 1978, *MNRAS* 184, 365
- Westerlund B.E., 1990, *A&AR* 2, 29
- Whiteoak, J. B. & Gardner, F. F. 1976, *MNRAS*, 174, 51
- Whiteoak, J. B., & Gardner, F. F. 1986, *MNRAS*, 222, 513
- Wiesenfeld, L., & Faure, A. 2013, *MNRAS*, 432, 2573
- Wienen, M., Wyrowski, F., Menten, K. M., et al. 2015, *A&A*, 579, 91
- Wienen, M., Wyrowski, F., Schuller, F., et al. 2012, *A&A*, 544, 146
- Wilson, T. L. & Rood, R. 1994, *ARA&A*, 32, 191
- Wong, T., Hughes, A., Ott, J., et al. 2011, *ApJS*, 197, 16
- Woon, D. 2002, *ApJ*, 569, 541
- Wouterloot, J. G. A., Henkel, C., Brand, J., Davis, G. R. 2008, *A&A*, 487, 237
- Yang, B., Stancil, P. C., Balakrishnan, N., & Forrey, R. C. 2010, *ApJ*, 718, 1062
- Zhang, J. S., Henkel, C., Mauersberger, R., et al. 2007, *A&A*, 465, 887
- Zhang, C., P., Esimbek, J., Zhou, J. J., et al. 2012, *Ap&SS*, 337, 283
- Zylka, R., Güsten, R., Henkel, C., & Batrla, W. 1992, *A&AS*, 96, 525